Eur. Phys. J. D **34**, 219–222 (2005)
DOI: 10.1140/epjd/e2005-00146-1

THE EUROPEAN PHYSICAL JOURNAL D

Formation of carbon-encapsulated metallic nano-particles from metal acetylides by electron beam irradiation

Ways for controlled patterning of metallic lines and magnetic dot arrays

J. Nishijo[1], C. Okabe[1], J. Bushiri[1], K. Kosugi[1], N. Nishi[1,a], and H. Sawa[2]

[1] Institute for Molecular Science, Myodaiji Nishigonaka 38, Okazaki 444-8585, Japan
[2] Institute of Material Structure Science, 1-1 Ohno, Tsukuba Ibaraki 305-0801, Japan

Received 6 September 2004
Published online 13 July 2005 –

Abstract. Transition metal acetylides, MC_2 (M=Fe, Co and Ni), exhibit ferromagnetic behavior of which T_C is characteristic of their size and structure. CoC_2 synthesized in anhydrous condition exhibited cubic structure with disordered C_2^{2-} orientation. Once being exposed to water (or air), the particles behave ferromagnetically due to the lengthening of the Co–Co distance by the coordination of water molecules to Co^{2+} cations. Heating of these particles induces segregation of metallic cores with carbon mantles. Electron beam or 193 nm laser beam can produce nanoparticles with metallic cores covered with carbon mantles.

PACS. 36.40.-c Atomic and molecular clusters – 36.40.Cg Electronic and magnetic properties of clusters – 36.40.Mr Spectroscopy and geometrical structure of clusters – 75.50.Tt Fine-particle systems; nanocrystalline materials

1 Introduction

In contrast to the S–S bonds in the transition-metal pyrite compounds (MS_2), the $C{\equiv}C^{2-}$ bonds of acetylide compounds (MC_2: M=Fe, Co and Ni) exhibit molecular-nature of the C_2^{2-} dianion. The orthogonal two π-orbitals of the dianion molecule are expected to strongly interact with *d*-orbitals of the transition-metal dication. The infrared absorption spectra of these acetylides show the C=C stretching vibrational bands in doublet in the same region as that of CaC_2. X-ray absorption near edge spectra of CoC_2 confirmed that the Co atom is in the dication state [1]. The magnetic and electronic properties of the acetylide compounds are very much related to geometrical configuration of metal atoms surrounded by C_2^{2-} dianions. Close location of the two metal atoms is prone to induce antiferromagnetic (AF) interaction, while ferromagnetic (FM) interaction is also expected for elongated metal-metal distances with the inserted molecule. We reported that CoC_2 is generated from the reaction of $Co_4(CO)_{12}$ with solvent CH_2Cl_2 not only by heating but also by UV irradiation [1,2]. In contrast to explosive property of M_2C_2 type acetylides such as Ag_2C_2 and Cu_2C_2, CoC_2 and NiC_2 are rather stable in atmospheric condition. Thus, one can make the transition metal acetylides efficiently through the ion exchange reaction of metal chloride with CaC_2 in dehydrated acetonitrile solution. The MC_2 compounds are expected to show CaC_2 type or MgC_2 type structure where metal cations and $C{\equiv}C^{2-}$ are alternatively stacked like a rock salt crystal, although the relative orientation of the anion molecule may depend on the synthetic condition. Closer location of the two metal atoms may induce AF interaction, while the elongation of the metal-metal distances may result in the FM interaction due to the elongated rhombus configuration of the M–C_2–M four-center unit. We demonstrate this property for CoC_2 nanocrystals synthesized at 78 °C. High temperature treatment of FeC_2, CoC_2, and NiC_2, however, induces charge neutralization resulting in the segregation of metal cores with graphitic or pyrolytic carbon mantles [3]. This phenomenon can be utilized for electron beam manufacturing of nano-dots or nano-wires on a Si substrate. VUV laser beam processing is also possible for acetylide thin layers.

2 Water induced structural change and ferromagnetism of CoC_2

Owing to the highly absorbency of CoC_2, ca. 1–2 H_2O molecules are coordinated to the Co^{2+} dication when CoC_2 is exposed to air or water. To investigate the influence of the coordinated water on the structure and magnetic property of CoC_2, XRD and SQUID measurement were done for hydrous and anhydrous CoC_2. Hydrous CoC_2 was prepared by the air exposure of

[a] e-mail: nishi@ims.ac.jp

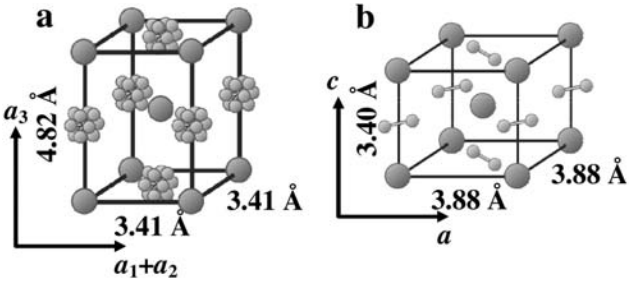

Fig. 1. The crystal structure of anhydrous (a) and hydrous (b) CoC_2. The figure of the anhydrous CoC_2 is a part of the fcc-unit cell. Large and small gray circles indicate cobalt and carbon atoms, respectively. The disorder of the C_2^{2-} dianions in anhydrous CoC_2 is depicted as a static disorder on several carbon positions.

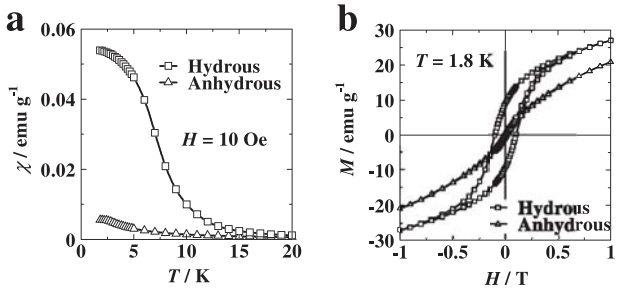

Fig. 2. Field-cooled magnetic susceptibility (a) and magnetization curves (b) of the anhydrous and hydrous CoC_2.

anhydrous CoC_2 for 2 hours. Though the washing with water also gives hydrous CoC_2 in a short time, air-exposed sample is suitable to measure the magnetic property thanks to its larger structural domain size.

The observed XRD pattern of the as-prepared anhydrous CoC_2, which is mostly originated from the scattering at the Co^{2+} dications, suggests the fcc-sublattice of Co^{2+} with the lattice constants $a_1 = a_2 = a_3 = 4.82$ Å. Judging from the crystal structures of CaC_2 and MgC_2, we expect that the Co^{2+} and C_2^{2-} ions form NaCl-like alternate stack, where the fcc arrangement of the Co^{2+} dications indicates the (static) orientation disorder of the C_2^{2-} dianions as shown in Figure 1a. The cubic structure involving the orientation disorder of C_2^{2-} dianions is also observed in CaC_2 at high temperature [4]. In addition, the small peak widths ($\Delta 2\theta \sim 2.00 \times 10^{-3}$ rad at $\theta = 24.0^{\circ}$, $\lambda = 0.9988$ Å) imply the large domain size D estimated as $D > 45$ nm by using Scherre's equation.

Although CoC_2 is water-stable material unlike CaC_2 and MgC_2, absorbed water changes the crystal structure of CoC_2 drastically. After air-exposure, the XRD peaks become broad and the positions change as Co^{2+} cations form the body-centered-tetragonal sublattice with the lattice constants $a = b = 3.88$, $c = 3.40$ Å. These values are consistent with the crystal structure forecasted from the EXAFS results ($a = b = 3.85$ Å and $c = 3.61$ Å), where the crystal structure of CoC_2 is regarded as the MgC_2-type structure [5] as shown in Figure 1b. In this phase, the a- and b-axes are expanded due to the absorbed waters coordinated to the Co^{2+}, while the c-axis becomes shorter. The orientation of the C_2^{2-} dianions are also affected by the lattice expansion and/or steric hindrance of the water, resulting in the structural change from the isotropic disordered orientation (Fig. 1a) to anisotropic ordered orientation (Fig. 1b). Because the structural change is too drastic to be done in concert, a CoC_2 particle is divided into many small domains. Indeed, the XRD peak widths of the hydrous CoC_2 $\Delta\theta \sim 1.25 \times 10^{-2}$ rad at $2\theta = 34.6^{\circ}$, $\lambda = 1.5418$ Å is remarkably larger than that of anhydride, suggesting the small domain size $D \sim 10$ nm of the hydrous CoC_2.

Inter-molecular magnetic interaction is sensitive to the arrangement of the molecules. Therefore, it is expected that the magnetism of the hydrous and anhydrous CoC_2 are largely different. Figure 2a shows the temperature dependence of the field-cooled magnetic susceptibilities χ of CoC_2 before and after the air-exposure measured at $H = 10$ Oe. It is noted that ICP measurement reveals the CoC_2 containing ca. 30 at% of starting material (CaC_2), therefore observed χ is probably ca. 30% smaller than that of pure CoC_2. χ of the anhydrous CoC_2 obeys the Curie-Weiss law in the high temperature range above ca. 70 K with Curie constant $C = 1.1$ emu K/mol and AF Weiss temperature $\Theta = -10$ K, the former of which is obviously larger than the value of Co^{2+} cation ($C = 0.375$), suggesting the short-range strong FM interaction. Below 2.5 K, the anhydrous CoC_2 shows ferromagnetism as discussed in later, but the FM part is only less than 8%.

Although χ of the hydrous CoC_2 also obeys the Curie-Weiss law above ca. 100 K, $C = 1.5$ emu K/mol is significantly larger than that of anhydrous CoC_2 suggesting the expansion of the FM domain, while AF $\Theta = -3$ K indicates the weakening of the AF interaction between FM domains. The difference of the magnetism between hydrous and anhydrous CoC_2 is evidently caused by the water-induced structural changes; that is, the orientation ordering of C_2^{2-} dianions and the change of the inter- and intra-chain distances. Judging from the fact that the interaction is weakened by lengthening the inter-molecular distance, we conclude that the AF and FM interactions are attributed to the inter- and intra-chain interaction. In the anhydrous phase, the orientation of C_2^{2-} dianions are disordered, resulting in the fragmental small FM domains owing to the disordered FM and AF interactions. On the other hand, the orientation of the C_2^{2-} dianions tends to be ordered in hydrous phase, where the FM interactions are connected to each other and form the FM chain elongated parallel to the c-axis, resulting in the large FM domains.

The water-induced ferromagnetism is clearly observed in the magnetization curves as shown in Figure 2b. In the case of anhydrous CoC_2, only a small amount of the FM component shows hysteresis loop with coercive force $H_C = 150$ Oe and remanent magnetization $M_{REM} = 0.7$ emu g^{-1}, while the greater part of CoC_2 behaves as paramagnet with weak AF interaction. The small amount of the FM component is perhaps caused by the residual water in the resin used for the SQUID measurement.

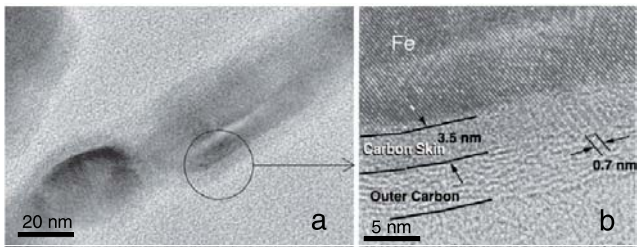

Fig. 3. TEM image of the Fe nano-rod (a) and its enlargement (b). Iron core is covered with the graphite skin whose thickness is ca. 3.5 nm (see text).

Contrary to the anhydrous CoC_2, the hysteresis loop of the hydrous CoC_2 is clearly observed with $H_c = 1000$ Oe and $M_{REM} = 9.0$ emu g^{-1}. The results clearly show the importance of the water in the ferromagnetism of CoC_2.

Here, we briefly note the effect of the water on FeC_2 and NiC_2. Anhydrous FeC_2 shows paramagnetism except a very small ferromagnetic part, as like as anhydrous CoC_2. However, different from CoC_2, water-absorption decomposes FeC_2 into acetylene and iron hydroxide like as CaC_2. In the case of NiC_2, the major part shows ferromagnetism even in anhydrous phase. Furthermore, water-absorption does not occur (or very slow) in NiC_2. The difference may be originated from the configuration of the *d*-electrons, but detail is still unclear.

3 Carbon-skinned Fe rods

By the rapid stirring of the acetonitrile solution with $FeCl_2$ and CaC_2 fine particles, one can get the Fe nanocrystals with graphitic carbon-skins. Carbon-protected metal nanoparticle is a promising material for magnetic devices owing to its chemical stability [6]. The reaction time should be as long as 48 hours at 250 °C. The intermediate product of FeC_2 shows charge neutralization reaction and segregation into metal and carbon components. Though bulk carbon and bulk iron are more stable than FeC_2, alternate stack of Fe^{2+} and C_2^{2-} forbids the neutralization at low temperature, where the neutral Fe-C_2 pair caused by electron transfer is re-ionized by Coulomb potential of adjacent ions. On the contrary to low temperature, neutral iron and carbon atoms can easily migrate and gather before re-ionization at high temperature. Once the "iron core" is formed, the core collects neighbouring iron atoms and becomes iron nanoparticle covered with residual carbon atoms. X-ray diffraction pattern of the products exhibits an asymmetric broad band at $2\theta = 26.0^{\circ}$ that was assigned to graphitic carbon. From the Scherrer equation, the average size of the iron core is estimated as 30 nm. Figure 3 shows the TEM images of a nano-rod with a neck. Figure 3b is an expanded image of the outer area. Although most of nano-crystals with short lengths exhibit single carbon-skin with a thickness of 3.5 nm, this long rod wears double carbon layers. The first skin layer is directly bonded with an iron metal core and the rod wears the second outer-mantle with planes parallel to the iron surface. The direct bonding of the graphitic axis to Fe axes was attributed to accidental coincidence of the Fe–Fe distance (2.866 Å) with the C_1–C_4 distance of a graphite hexagonal ring (2.842 Å). Due to the modification of the surface structure, the saturation magnetization at 300 K of the carbon-skinned Fe nano-particles with an average diameter of 60 nm was as high as 80% of that at 1.8 K [3].

The carbon-skinned metal nanoparticles of Co and Ni can also be obtained from acetylide, but the "skin" is amorphous carbon due to the lattice mismatch between graphite and Ni or Co metals.

The second ionization potentials of Ni, Co, and Fe are 18.1688, 17.083, and 16.1878 eV, respectively, and the first ionization potentials are 7.6398, 7.8810, and 7.9024 eV, respectively [7].

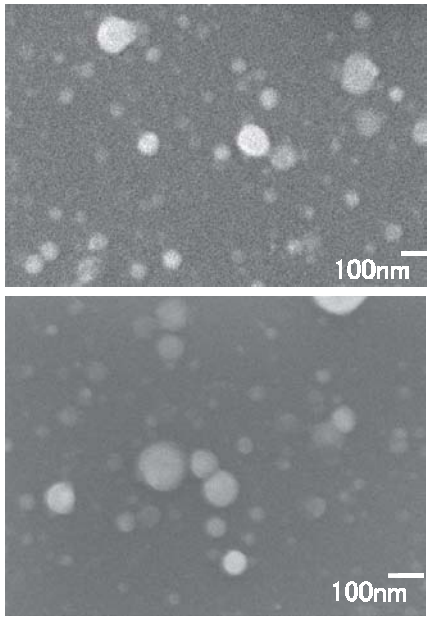

Fig. 4. Typical SEM images of the carbon-encapsulated Co nanoparticles formed by 193 nm laser irradiation on CoC_2 in Ar atmosphere (0.5 torr).

4 Carbon-encapsulated Co by VUV irradiation of CoC_2

Because of its water- and air-stability, CoC_2 is suitable to create a thin film of carbon-encapsulated metal nanoparticles by laser irradiation, where we must treat a bulk amount of the material. CoC_2 disk is irradiated by a 193 nm ArF laser beam in Ar atmosphere. The particles sputtered from the surface were deposited on a Si(111) surface. Figure 4 shows typical SEM images of the surface. White particles are somewhat charged up due to the insulation by the carbon mantle of the spheric particles with Co cores. EDS analysis reveals that the particles consist of carbon and cobalt atoms. These figures demonstrate that 193 nm laser beam irradiation produces carbon-encapsulated spherical Co particles. The size of the particles are dependent on the laser power. Higher intensity causes larger particles. For the generation of the

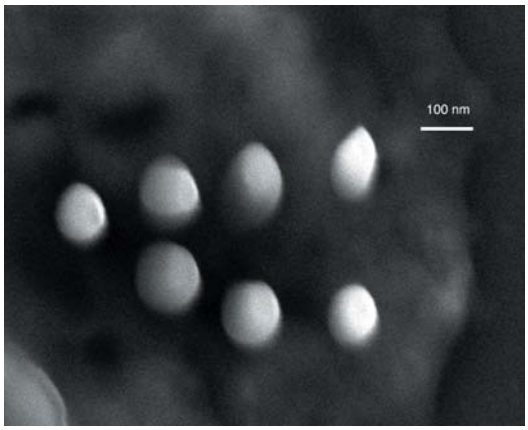

Fig. 5. Nickel nanodots from NiC_2 formed by the electron beam irradiation.

particles in Figure 4 we controlled the laser power as high as 200 mJ/cm^2.

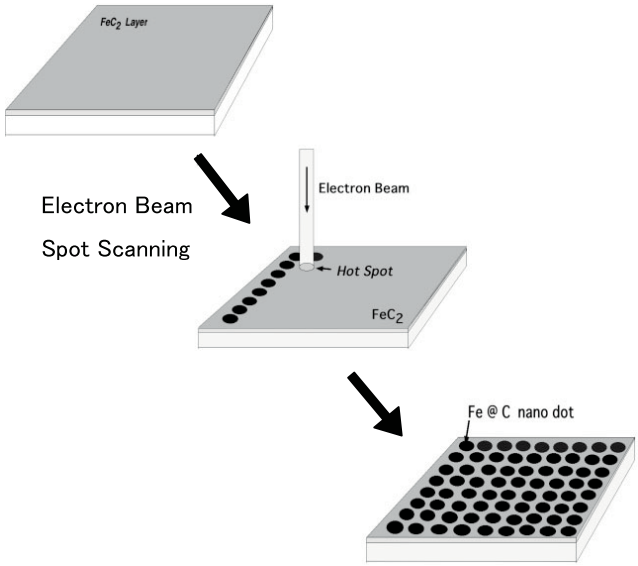

Fig. 6. Schematic illustration of the nano-dots arrays formation by electron beam heating.

5 Nano-dots formation by electron beam heating of NiC_2

Spot irradiation of weak electron beams can generate the metallic dots covered with carbons. Figure 5 shows an example of the preparation of nickel particles with carbon mantles with a scanning electron microscope (SEM), where we used NiC_2 because of its lower segregation temperature (150 °C) than that of CoC_2 or FeC_2 (> 200 °C). The lower segregation temperature is owing to the large second ionization potentials of Ni [7], and is suited to create a dot by weak electron beam. In the creation of dot, NiC_2 flat particles were situated on a Si(100) surface. Electron beam current was adjusted to 8 pA and irradiation was performed at arbitrary points. The size of the white spots became larger with elongating irradiation time and grew up to 100 nm after 3 minutes. The shape of the spots reflects the flatness of the surface. Appearance of white spots suggests that the carbon mantles on the metallic cores are very poor electric conductors and charges are localized on the surface of the amorphous carbon mantle. The observation of the energy dispersive X-ray spectrum suggested that the yield of carbon signals relative to that of Ni increases with increasing irradiation time. This indicates that the metallic core as well as the thickness of the carbon mantle grows with elongated heating time. NiC_2, in particular, is easily segregated even during the SEM image observations when electron beam current is not weakened.

This phenomenon can be applied for making nano-dots arrays embedded in an acetylide matrix. Figure 6 illustrates how to make nano-dots arrays on a silicon surface. Acetylide thin layer can be made in diluted Ar atmosphere by 193 nm laser sputtering at a moderate photon flux. The acetylide layer is composed of minute particles with diameters of sub-nanometer or nanometers. These tiny acetylide particles are superparamagnetic and, therefore, they can shield the magnetic moment of the magnetic dots. This role is very important, since the magnet-magnet interaction between the big dots is so large that the memory written in each dot can be easily destroyed through this interaction. The insulation by the surrounding tiny paramagnets from the strong inter-magnet interaction is quite necessary for the stabilization of the magnetic moments of the dots. For the dots larger than 200 nm, the direct heating can be done with focused 193 nm beam through a mask pattern. Carbon-covered Co spherical-dots with diameters of order of several hundred nm were formed with focused 193 nm laser irradiation on CoC_2 disks. This indicates that laser irradiation can melt CoC_2 and segregate Co cores as aligned magnets.

References

1. N. Nishi, K. Kosugi, K. Hino, T. Yokoyama, E. Okunishi, Chem. Phys. Lett. **369**, 198 (2003)
2. N. Nishi, K. Kosugi, K. Hino, T. Yokoyama, Eur. Phys. J. D **24**, 97 (2003)
3. K. Kosugi, M.J. Bushiri, N. Nishi, Appl. Phys. Lett. **84**, 1753 (2004)
4. M. Knapp, U. Ruschewitz, Chem. Eur. J. **7**, 874 (2001)
5. P. Karen, A. Kjekshus, Q. Huang, V.L. Karen, J. Alloy Comp. **282**, 72 (1999)
6. A.-H. Lu, W.-C. Li, N. Matoussevitch, B. Spliethoff, H. Bönnemann, F. Schüth, Chem. Commun. (2005), DOI:10.1039/b414146f
7. *CRC handbook of Chemistry and Physics*, edited by D.R. Linde, 75th edn. (CRC Press, Inc., Boca Raton, Florida, 1994), Chap. 10, p. 205